(iii) Because the information distinguishing structures such as those in Figs. 1 and 2 will mainly reside in small intensity differences at high $(\sin\theta)/\lambda$, accurate determinations of absolute magnitudes for all odd-order anharmonic parameters are more likely to be achieved with neutron-diffraction techniques. A further inherent advantage of neutron diffraction is the possibility of maximizing the difference in magnitude of the scattering lengths by varying the isotopic proportions of the atoms in a structure.

Finally, a note of caution. When fourth-order terms (C_i^{jklm}) are included in our $PbTiO_3$ refinements, parameter correlations arise which reduce the accuracy with which the C^{113} and C^{333} quasi-moments are determined. This highlights the need always to test for significant fourth-order terms in studies of skewness: such terms may substantially increase the demands on data accuracy and resolution relative to the intrinsic 'distinguishability' of the skewness.

We are grateful for a number of helpful discussions about anharmonic structure refinement with W. F. Kuhs, who has also played a large part in the collection and analysis of the $PbTiO_3$ data. The work is part of a research programme funded by the Science and Engineering Research Council.

References

DUCKWORTH, J. A. K., WILLIS, B. T. M. & PAWLEY, G. S. (1970). *Acta Cryst.* A**26**, 263-271.

HAZELL, R. G. & WILLIS, B. T. M. (1978). *Acta Cryst.* A**34**, 809-811.

JOHNSON, C. K. & LEVY, H. A. (1974). *International Tables for X-ray Crystallography*, Vol. IV, pp. 311-336. Birmingham: Kynoch Press. (Present distributor D. Reidel, Dordrecht.)

KUHS, W. F. (1983). *Acta Cryst.* A**39**, 148-158.

MOSS, B., MCMULLAN, R. K. & KOETZLE, T. F. (1980). *J. Chem. Phys.* **73**, 495-508.

NELMES, R. J. & KUHS, W. F. (1985). *Solid State Commun.* **54**, 721-723.

SHIRANE, G. & HOSHINO, S. (1951). *J. Phys. Soc. Jpn*, **6**, 265-270.

YAMANAKA, T. & TOKONAMI, M. (1985). *Acta Cryst.* B**41**, 298-304.

ZUCKER, U. H., PERENTHALER, E., KUHS, W. F., BACHMANN, R. & SCHULZ, H. (1983). *J. Appl. Cryst.* **16**, 358.

Acta Cryst. (1987). A**43**, 638-645

Resolution Analyses for Mössbauer Diffraction: Resolved TDS Profiles in Silicon*

BY M. L. CROW, G. SCHUPP AND W. B. YELON

Research Reactor and Department of Physics, University of Missouri, Columbia, MO 65211, *USA*

AND J. G. MULLEN AND A. DJEDID

Department of Physics, Purdue University, West Lafayette, IN 47907, *USA*

(*Received* 2 *January* 1987; *accepted* 31 *March* 1987)

Abstract

The resolution function for Mössbauer γ-ray scattering and the thermal diffuse scattering (TDS) near the 444 reflection in silicon have been measured with high-intensity Mössbauer radiation from the 46·48 keV transition in ^{183}W. A general analysis of the resolution function has been carried out for the first time which shows that its energy and momentum components can be factored independently with the energy resolution being determined by the Mössbauer resonance. The half-widths of the momentum resolution ellipsoid were measured to be 0·011, 0·11 and 1·13 $Å^{-1}$ in the transverse, longitudinal and vertical directions, respectively. The ratios of these half-widths are significantly different from those commonly encountered in neutron scattering. These analyses indicate that the observed broad distribution of inelastic scattering in the TDS profiles is consistent with published elastic constants for silicon.

Introduction

Thermal diffuse scattering (TDS) is coherent inelastic scattering due to lattice vibrations in a crystalline solid. In a conventional X-ray diffraction experiment, the TDS, with energy transfer of 0-0·1 eV, is not directly separable from the Bragg scattering intensity, since these energy shifts are smaller than the 1-5 eV intrinsic energy spread of common X-ray lines. The

* This material was prepared with the support of the US Department of Energy, Grant Nos. DE-AC02-83ER 45017, DE-FG02-85ER 45200, and DE-FG02-85ER 45199 A00. However, any opinions, findings, conclusions or recommendations expressed herein are those of the authors and do not necessarily reflect the views of DOE.

0108-7673/87/050638-08$01.50

TDS has a maximum intensity at the reciprocal-lattice points, thus adding to the apparent intensities of the Bragg peaks. In systems where the TDS intensity is a significant fraction of the elastic intensity, a knowledge of the TDS becomes essential for the determination of accurate temperature factors and detailed electron-density distributions. The TDS contribution can be calculated if the phonon dispersion relations and the volume observed in reciprocal space are known. The TDS contributions for a number of specific types of scans around the reciprocal-lattice point have been calculated (Nilsson, 1957; Cooper & Rouse, 1968; Willis, 1969) with sound velocities averaged over all directions.

In order to measure the TDS contribution experimentally, the elastic scattering must be separated from the inelastic scatteing. The small energy width of Mössbauer lines suggests a direct method of measuring the elastic scattering fraction, since inelastic scattering of energy transfer larger than the resonant width is not absorbed resonantly (O'Connor & Butt, 1963). Several Mössbauer scattering studies of TDS in silicon have been performed with the 14·4 keV transition in ^{57}Fe (Ghezzi, Merlini & Pace, 1969; Albanese, Ghezzi, Merlin & Pace, 1972; Kashiwase & Minoura, 1983; Krec & Steiner 1984). Owing to the low intensities available from the ^{57}Co sources, these experiments were run with large angular divergences (low momentum resolution), in order to obtain adequate counting rates. Thus the observed TDS intensities in these earlier studies represented an integration over a large fraction of the Brillouin zone. The development of γ-ray diffraction instruments using intense sources (Schneider, 1974, 1983; Yelon & Ross, 1982) led to the construction of a high-intensity Mössbauer scattering instrument (Yelon, Schupp, Crow, Holmes & Mullen, 1986), which has allowed the TDS to be observed with much higher momentum resolution. These measurements have given motivation for a resolution-function analysis, analogous to the general procedure presented by Cooper & Nathans (1967) for neutron diffraction, appropriate for Mössbauer γ-ray scattering.

Experiment

The vibrational spectrum of silicon has been studied extensively by a variety of techniques. The dispersion curves have been mapped by thermal neutron scattering and modeled theoretically (Dolling & Cowley, 1966; Nilsson & Nelin, 1972), so that the momentum dependence of the vibrational spectrum is very well known. In addition, large perfect crystals are readily available, making silicon a convenient sample for evaluating a TDS separation method. Perfect crystals were desirable for this type of experiment because the very narrow elastic Bragg peak allowed the TDS to be observed more easily. The sample in this study was a $5{\cdot}5\times3{\cdot}0\times0{\cdot}6$ cm perfect silicon crystal, cut parallel to the (220) lattice planes.

The γ-ray diffractometer at the University of Missouri Research Reactor, QUEGS (quasi-elastic gamma-ray scattering), uses an intense Mössbauer source cooled to 77 K. The 46·48 keV transition in ^{183}W (from the decay of ^{183}Ta) was used in this study. Nominal 70 Ci (1 Ci = 37 GBq) sources were produced by one-week irradiations in the flux trap of the University of Missouri Research Reactor, which has a thermal flux of 4×10^{14} neutrons cm^{-2} s^{-1}, by successive neutron capture from ^{181}Ta. A LiF(200) crystal monochromating filter was used to reduce background by preventing other γ-rays and X-rays present in the source from reaching the sample position, as shown in Fig. 1. The sample was mounted on a rotary stage in symmetric Laue geometry. Four absorbers of enriched ^{183}W metal powder in a plastic matrix were mounted in a paddle-wheel arrangement on a vertical-axis rotor. These absorbers could be driven at constant velocities ranging from 0·64 to 320 cm s^{-1}, giving an appropriate velocity range for the very broad 46·48 keV Mössbauer transition, which has a natural width of 3·2 cm s^{-1} (Lederer & Shirley, 1978). The detector was a 2·5 cm diameter × 1 cm thick intrinsic Ge detector, which provided nearly 100% efficiency at 46·48 keV. In addition, the 1 keV energy resolution given by the detector allowed good separation of the resonant and non-resonant 46·48 keV γ-rays from other γ- and X-rays, with a single-channel analyzer.

After each irradiation the sources were cooled to liquid-nitrogen temperature, and the intensities of the γ-rays scattered from the LiF crystal were measured at a range of absorber velocities. Because of the large elastic constants of LiF and the use of a low-angle

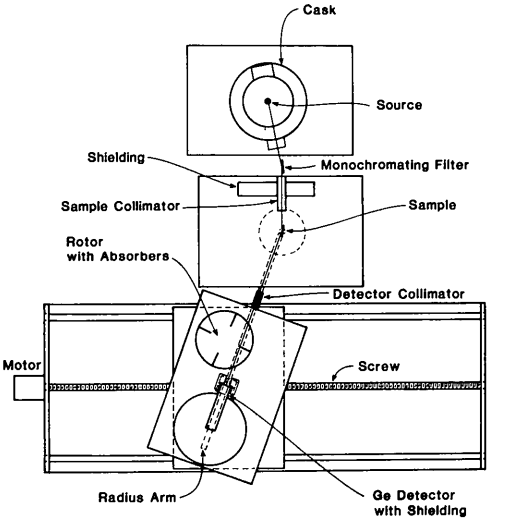

Fig. 1. Schematic drawing of the QUEGS instrument. A radius arm pivoted at the sample axis keeps the detector collimator precisely directed towards the sample as 2θ is changed.

reflection, the scattering observed for the LiF(200) Bragg peak is essentially 100% elastic (Mullen & Stevenson, 1978), providing a convenient standard for determination of source and absorber resonance characteristics. The parameters of the resonance were determined by fitting the observed absorption curve to a Lorentzian shape using a least-squares procedure. The resonance absorption fraction $P_{el}(0)$ observed for the elastic LiF(200) peak is defined by

$$P_{el}(0) = [I(\infty) - I(0)]/[I(\infty) - B], \qquad (1)$$

where $I(\infty)$ is the counting rate for an infinite absorber velocity, $I(0)$ is the counting rate for a zero absorber velocity, and B is the background counting rate. Typical resonance curves yielded a value for $P_{el}(0)$ of 0·27 and an experimental width of 5·5 cm s^{-1}. Preliminary scans to align the crystal were performed while moving the absorbers at a constant velocity (19·2 cm s^{-1}) far greater than the resonance width. Since the 'paddle-wheel' absorber arrangement produced a variable absorber thickness, all counting times corresponded to an integral number of rotor revolutions, which required the use of a non-zero on-resonance velocity. The isomer shift of the resonance was found to be about 1% of the line width and has been neglected in this analysis. The elastic and inelastic scattering near the silicon 444 reflection were measured using an 'on-off' method, where the instrument alternately counted at a velocity v_l of 0·64 cm s^{-1}, well within the resonance width, and at a velocity v_h of 19·2 cm s^{-1}, about six times the natural line width. The elastic fraction was determined by

$$R_{el} = \frac{1}{P_{el}(0)} \frac{a}{b} \frac{I(v_h) - I(v_l)}{I(v_h) - B} \qquad (2)$$

where $I(v_h)$ was the intensity observed at the 'off-resonance' velocity and $I(v_l)$ was the intensity at the 'on-resonance' velocity. The ratios a and b, given by

$$a = [I(\infty) - I(0)]/[I(v_h) - I(v_l)] \qquad (3)$$

and

$$b = [I(\infty) - B]/[I(v_h) - B], \qquad (4)$$

are correction factors determined from the Lorentzian fit to the absorption curve, which account for the non-zero and finite values of the counting velocities. The relative intensities I_{el} and I_{in} for elastic and inelastic scattering can then be determined from

$$I_{el} = a[I(v_h) - I(v_l)] \qquad (5)$$

$$I_{in} = P_{el}(0)b[I(v_h) - B] - I_{el}. \qquad (6)$$

The background B was determined by two methods. In the first, the silicon crystal was rotated approximately 5° from the Bragg-angle setting. This method had the disadvantage that the TDS intensity at this angle was included, but this intensity was expected to be very low because of the high momentum resolution. In the other method, a 0·075 cm thick Cd foil was placed between the source and the monochromator. This thickness was enough to attenuate 99·997% of the 46·48 keV intensity, but allowed higher-energy photons to reach the sample and detector. Since the two methods agreed, it was evident that the principal source of background was Compton scattering and fluorescence radiation entering the single-channel analyzer window due to the interaction of the higher-energy γ-rays with the lead shielding. In both cases, the background could be separated into a component which decayed with the 5·1 day ^{183}Ta activity, and a nearly constant component due to the 115 day ^{182}Ta activity and room background.

Data were collected for points near the (444) reciprocal-lattice point. Fig. 2 shows a series of points in a θ scan. The elastic intensities were fitted to a Gaussian profile, giving a resolution half-width of 0·011 Å^{-1} in this direction, transverse to the scattering vector **Q**. Within the elastic half-width, the inelastic intensities decrease slowly with increasing $\mathbf{q} = \mathbf{Q} - \mathbf{G}$, the distance from the Bragg peak. Fig. 3 shows a θ-2θ scan parallel to **Q**. The resolution half-width here is ten times broader at 0·11 Å^{-1}, and the greater decrease in the inelastic scattering shown here is due principally to the larger **q** range. The θ-2θ scan was repeated with a 25% larger LiF monochromating crystal to increase the intensity, causing a change in resolution width. The solid circles are the elastic data with the smaller LiF crystal, and the open circles are the corresponding inelastic data. The solid squares are the elastic data with the larger LiF crystal, and

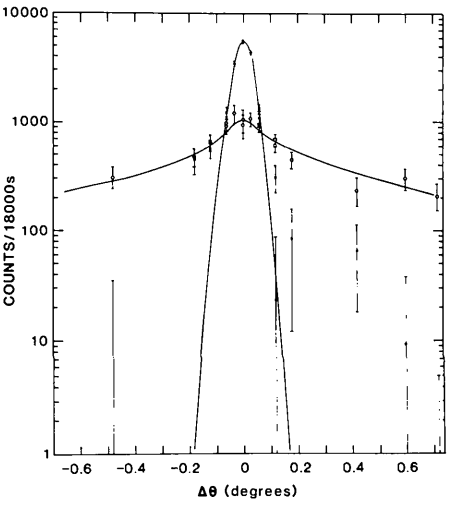

Fig. 2. Elastic (closed circles) and inelastic (open circles) scattering intensities for a θ (transverse) scan through the 444 Bragg reflection in silicon. The line through the elastic points is a Gaussian, and the line through the inelastic points was determined by the numerical integration procedure described in the analysis section of the text.

the Gaussian is from a least-squares fit to these points. The difference in width between the two sets of data for the elastic peak is readily apparent. The open squares are the inelastic data collected with the larger LiF crystal, and the calculated inelastic intensity profile shown here has been calculated for the resolution volume of this second scan. For the inelastic intensity profiles, the difference between these two cases was not evident in these data.

Analysis

For the QUEGS instrument, the incident beam originates in the ^{183}Ta source. The resonant part of the 46·48 keV intensity has an intrinsic width of 5 μeV, and the non-resonant part is broadened through phonon processes in Ta. The LiF monochromating filter prevents radiation of other energies present in the source spectrum from reaching the sample. This means that, in contrast to monochromators in neutron and X-ray instruments, the monochromating filter in QUEGS does not determine the energy distribution of the incident beam. This fact is the departure point for the resolution-function analyses presented here for Mössbauer diffraction.

Since $\Delta E/E$ is 10^{-10} (5 μeV/50 keV) for the incident beam, and only of order 10^{-6} between the incident and final TDS-shifted energies, the incident and final wave vectors $\mathbf{k}_i$ and $\mathbf{k}_f$ can be considered to be of equal magnitude and to form the surface of a sphere, as shown in Fig. 4 for the scattering geometry used in these analyses. A particular instrumental setting determines the initial and final wave vectors, $\mathbf{k}_i^0$ and $\mathbf{k}_f^0$, which are related to the scattering vector $\mathbf{Q}^0$ by $\mathbf{Q}^0 = \mathbf{k}_f^0 - \mathbf{k}_i^0$. These vectors all lie in the xy scattering plane, with $\mathbf{Q}^0$ being parallel to the x direction and perpendicular to the y direction. Angles measured within the scattering plane are denoted by θ and angles in directions perpendicular to the plane are denoted by φ.

If we recall that $E_i = (h/2\pi)\omega_i = (h/2\pi)ck_i$, with $k_i = |\mathbf{k}_i|$, the photon number distribution as a function of wave vector in the incident beam may be written as

$$s(k_i) = s_n(k_i) + s_r(k_i), \tag{7}$$

where $s_n(k_i)$ and $s_r(k_i)$ are the non-resonant and resonant components, respectively. The resonant component, $s_r(k_i)$, is a Lorentzian distribution of photons centered at the transition energy with a 5 μeV width. The total flux of γ-rays at the sample ($\mathrm{cm}^{-2}\,\mathrm{s}^{-1}$) is defined by $\Phi_{\text{total}} = \Phi^0 \int s(k_i)\,\mathrm{d}k_i$, where Φ^0 is a normalizing flux proportional to source strength. The distribution function for the photons incident upon the sample becomes

$$\begin{aligned} P_m(\mathbf{k}_i) &= P_m(k_i, \theta_i, \varphi_i) \\ &= [s_n(k_i) + s_r(k_i)] \exp\left(-\tfrac{1}{2}\{[(\theta_i - \theta_i^0)/\alpha_i]^2 \right. \\ &\quad \left. + [(\varphi_i - \varphi_i^0)/\beta_i]^2\}\right), \end{aligned} \tag{8}$$

where the horizontal and vertical divergences are approximated as Gaussian distributions characterized by the parameters α_i and β_i, respectively, in the manner of Cooper & Nathans (1967). The probability

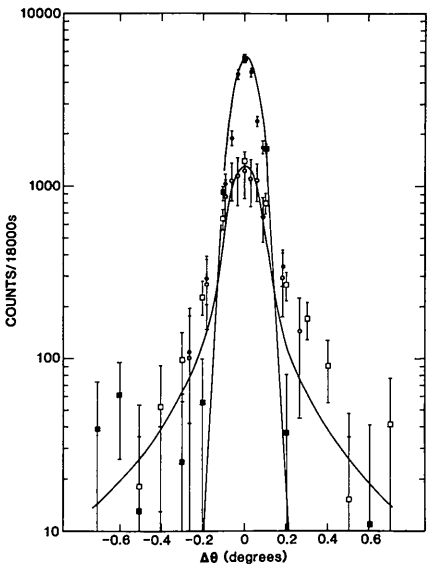

Fig. 3. Elastic (closed circles) and inelastic (open circles) scattering intensities are shown for a θ-2θ (longitudinal) scan through the silicon 444 with the smaller of the two LiF monochromating-filter crystals. Also shown are the elastic (closed squares) and the inelastic (open squares) scattering intensities for a similar scan with the larger LiF monochromating-filter crystal. The line through the elastic scan with the larger LiF crystal is a Gaussian, and the line through the inelastic points was determined by the numerical integration procedure described in the analysis section of the text.

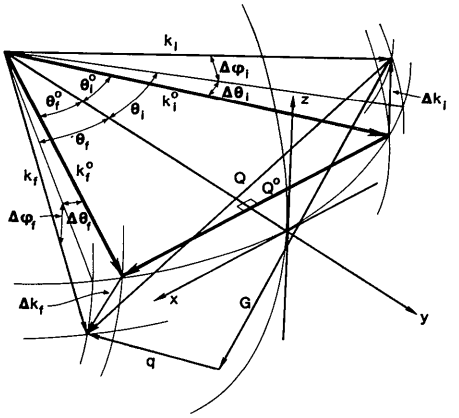

Fig. 4. An illustration of a γ-ray scattering experiment in reciprocal space. The symbols are defined in the text. While $\mathbf{k}_i^0$ and $\mathbf{k}_f^0$ appear to be different in the projection shown here, they are actually equal in magnitude.

of counting the scattered γ-rays is

$$P_d(\mathbf{k}_f) = P_d(k_f, \theta_f, \varphi_f) = A(k_f) \exp\left(-\tfrac{1}{2}\{[(\theta_f - \theta_f^0)/\alpha_f]^2 + [(\varphi_f - \varphi_f^0/\beta_i]^2\}\right), \quad (9)$$

where θ_f^0 is the angle in the scattering plane between $\mathbf{k}_f^0$ and the perpendicular to $\mathbf{Q}^0$, φ_f^0 is zero, and α_f and β_f are Gaussian parameters describing the horizontal and vertical divergences of the detector. The absorber-detector acceptance function $A(k_f)$ is determined by the efficiency of the detector and the attenuation by the rotor, and is written (Mullen, Djedid, Holmes, Schupp, Crow & Yelon, 1986)

$$A(k_f) = \varepsilon \int_0^t \exp\left[-\sum_i \sigma_{e_i} N_i t' - \sigma_r(k_f) f_a N_0 t'\right] dt', \quad (10)$$

where ε is the detector efficiency, σ_{e_i} is the photoelectric absorption cross section and N_i is the number density of each atomic species in the absorber; t is the absorber thickness. The resonant absorption cross section $\sigma_r(k_f)$ has a Lorentzian dependence on the rotor velocity, f_a is the recoilless fraction, and N_0 is the number density of Mössbauer atoms in the absorber. The observed counting rate I is then given by the integral

$$I = c\Phi^0 \int P_m(k_i, \theta_i, \varphi_i)(d^2\sigma/d\omega\, d\Omega) P_d(k_f, \theta_f, \varphi_f) \times \cos\varphi_i \cos\varphi_f\, dk_i\, dk_f\, d\theta_i\, d\theta_f\, d\varphi_i\, d\varphi_f, \quad (11)$$

where $d^2\sigma/d\omega\, d\Omega$ is the double differential scattering cross section of the sample, and c is the velocity of light. Within the angular resolution of the instrument, the components of the general scattering vector $\mathbf{Q} = \mathbf{k}_f - \mathbf{k}_i$ can be written

$$Q_x = k_f \sin\theta_f \cos\varphi_f - k_i \sin\theta_i \cos\varphi_i \quad (12a)$$

$$Q_y = k_f \cos\theta_f \cos\varphi_f - k_i \cos\theta_i \cos\varphi_i \quad (12b)$$

$$Q_z = k_f \sin\varphi_f - k_i \sin\varphi_i, \quad (12c)$$

and the energy transfer is

$$(h/2\pi)\omega = (h/2\pi)ck_f - (h/2\pi)ck_i. \quad (12d)$$

Since the change in the scattering-vector magnitude is very small in γ-ray scattering, $k_f^0 = k_i^0 = k^0$, and $\theta_f^0 = -\theta_i^0 = \theta^0$. Then the components of $(\mathbf{Q}^0, \omega^0)$ become

$$Q_x^0 = 2k^0 \sin\theta^0 \quad (13a)$$

$$Q_y^0 = Q_z^0 = 0 \quad (13b)$$

and

$$\omega^0 = 0. \quad (13c)$$

Since $\Delta\varphi_i$, $\Delta\varphi_f$, $\Delta\theta_i$ and $\Delta\theta_f$ are small angles, the approximations that $\sin\Delta = \Delta$ and $\cos\Delta = 1$ are valid. As mentioned earlier, since $\Delta k_i/k^0$ and $\Delta k_f/k^0$ are of the order 10^{-6} or less, Δk_f and Δk_i can be neglected relative to k. Under these approximations, it follows that

$$\Delta Q_x = Q_x - Q_x^0 = k^0 \cos\theta^0(\Delta\theta_f - \Delta\theta_i) \quad (14a)$$

$$\Delta Q_y = Q_y - Q_y^0 = k^0 \sin\theta^0(\Delta\theta_f + \Delta\theta_i) \quad (14b)$$

$$\Delta Q_z = Q_z - Q_z^0 = k^0(\Delta\varphi_f - \Delta\varphi_i) \quad (14c)$$

$$\Delta\omega = \omega - \omega^0 = c(\Delta k_f - \Delta k_i). \quad (14d)$$

With these expressions, (11) can be rewritten in the form

$$I = [\Phi^0/(k^0)^3 \sin 2\theta^0] \times \iint (d^2\sigma/d\omega\, d\Omega) R(\Delta\mathbf{Q}, \Delta\omega)\, d^3\Delta\mathbf{Q}\, d\Delta\omega, \quad (15)$$

where $R(\Delta\mathbf{Q}, \Delta\omega)$ is the instrumental resolution function, which is defined by

$$R(\Delta\mathbf{Q}, \Delta\omega) = \iint P_m(k_i, \theta_i, \varphi_i) \times P_d(k_f, \theta_f, \varphi_f)\, d\Delta\varphi_i\, d\Delta k_i. \quad (16)$$

This resolution function describes the volume in momentum space and the range of energy in which scattering processes can contribute to the observed intensity for a given instrumental setting. The resolution function can be separated into horizontal, vertical and energy components, to give

$$R(\Delta\mathbf{Q}, \Delta\omega) = H(\Delta Q_x, \Delta Q_y) V(\Delta Q_z) E(\Delta\omega), \quad (17)$$

where

$$H(\Delta Q_x, \Delta Q_y) = \exp\{-\tfrac{1}{2}[(\Delta\theta_i/\alpha_i)^2 + (\Delta\theta_f/\alpha_f)^2]\}$$

$$V(\Delta Q_z) = \int \exp\{-\tfrac{1}{2}[(\Delta\varphi_i/\beta_i)^2 + (\Delta\varphi_f/\beta_f)^2]\}\, d\Delta\varphi_i$$

and

$$E(\Delta\omega) = \int [s_n(k_i) + s_r(k_i)] A(k_f)\, d\Delta k_i.$$

First, consider the horizontal component H. From (14a) and (14b),

$$\Delta\theta_i = -\tfrac{1}{2}[(\Delta Q_x/k^0 \cos\theta^0) + (\Delta Q_y/k^0 \sin\theta^0)] \quad (18a)$$

$$\Delta\theta_f = \tfrac{1}{2}[(\Delta Q_x/k^0 \cos\theta^0) - (\Delta Q_y/k^0 \sin\theta^0)]. \quad (18b)$$

Then

$$H = \exp\{-\tfrac{1}{2}[M_{11}\Delta Q_x^2 + M_{22}\Delta Q_y^2 + (M_{12} + M_{21})\Delta Q_x \Delta Q_y]\}, \quad (19)$$

where

$$M_{11} = \tfrac{1}{4}[1/(k^0)^2 \cos^2\theta^0][(1/\alpha_i)^2 + (1/\alpha_f)^2]$$

$$M_{22} = \tfrac{1}{4}[1/(k^0)^2 \sin^2\theta^0][(1/\alpha_i)^2 + (1/\alpha_f)^2]$$

$$M_{12} = M_{21} = \tfrac{1}{4}[1/(k^0)^2 \sin\theta^0 \cos\theta^0] \times [(1/\alpha_i)^2 - (1/\alpha_f)^2].$$

The vertical component can be evaluated by substitut-

ing $\Delta\varphi_f = \Delta Q_z/k^0 + \Delta\varphi_i$ into the expression

$$V(\Delta Q_z) = \int \exp\{-\tfrac{1}{2}[\Delta\varphi_i^2(1/\beta_i^2 + 1/\beta_f^2) + \Delta\varphi_i(2\Delta Q_z/\beta_f^2 k^0) + \Delta Q_z^2/\beta_f^2(k^0)^2]\}\, d\Delta\varphi_i. \quad (20)$$

The vertical component of the resolution is then

$$V(\Delta Q_z) = (2\pi\beta_i^2\beta_f^2/\beta_i^2 + \beta_f^2)^{1/2} \exp(-\tfrac{1}{2}M_{33}\,\Delta Q_z^2), \quad (21)$$

where

$$M_{33} = 1/(k^0)^2(\beta_i^2 + \beta_f^2).$$

The resolution effects described so far are features of the instrument itself, independent of details of the sample. The observed momentum resolution for a single crystal also depends on the horizontal and vertical mosaic spreads η_h and η_v. As discussed by Werner & Pynn (1971), mosaic has the effect of changing the M_{ij} of (19) and (21) to

$$M'_{ij} = M_{ij} - M_{i2}M_{j2}/[(1/\eta_h Q^0)^2 + M_{22}] \quad (22a)$$

for $i, j = 1, 2$ and

$$M'_{33} = M_{33} - M_{33}^2/[(1/\eta_v Q^0)^2 + M_{33}] \quad (22b)$$

for $i = j = 3$.

The resolution function in momentum may now be written

$$R(\Delta\mathbf{Q}) = \exp\left(-\tfrac{1}{2}\sum_{kl} M'_{kl}\,\Delta Q_k\,\Delta Q_l\right), \quad (23)$$

where $M'_{13} = M'_{31} = M'_{32} = 0$. This function describes a volume in momentum space which can be visualized as a three-dimensional ellipsoid with Gaussian half-width parameters.

Evaluation of $E(\Delta\omega)$ is mathematically more complex, because details of the source and absorber must be included. If (from 14d) $\Delta k_f = \Delta\omega/c + \Delta k_i$ is substituted into the expression for $E(\Delta\omega)$, it becomes

$$E(\Delta\omega) = \int [s_n(\Delta k_i) + s_r(\Delta k_i)]A(\Delta\omega/c + \Delta k_i)\, d\Delta k_i. \quad (24)$$

Although this integral can be evaluated numerically (Mullen *et al.*, 1987) it is operationally most appropriate to represent $E(\Delta\omega)$ by the measured line shape which in the present case can be fitted adequately by the Lorentzian

$$E(\Delta\omega) = C - D/[1 + X^2(\Delta\omega^0)], \quad (25)$$

where C and D are constants determined respectively by the source line shape and recoilless fraction, and by the photoelectric and resonant absorber cross sections, and

$$X(\Delta\omega^0) = (h/2\pi)(\Delta\omega - \Delta\omega^0)/(\Gamma_{\rm exp}/2), \quad (26)$$

where $\Gamma_{\rm exp}$ is the experimental line width, and $\Delta\omega^0$ is the effective center of the resonance, which can be changed by varying the rotor velocity. For very accurate evaluations of elastic intensity it is necessary to consider a more precise representation of the line shape than given by the Lorentzian used above.

The effective elastic-energy resolution function of the on-off method is expressed in terms of equation (25) by

$$E_{\rm el}(\Delta\omega) = aD\{1/[1 + X^2(v_l)] - 1/[1 + X^2(v_h)]\}. \quad (27)$$

The first term corresponds to scattering of zero energy transfer. The second term includes the small fraction of the total inelastic scattering which is within the window at $v_h = 19{\cdot}2$ cm s^{-1}, corresponding to an energy transfer of 30 μeV. The corresponding expression for the inelastic scattering is

$$E_{\rm in}(\Delta\omega) = bP_{\rm el}(0)C - aD/[1 + X^2(v_l)] + [a - bP_{\rm el}(0)]D/[1 + X^2(v_h)]. \quad (28)$$

Since the value of $1/[1 + X^2(v_h)]$ is small, the expressions become

$$E_{\rm el}(\Delta\omega) = aD/[1 + X^2(v_1)] \quad (29)$$

and

$$E_{\rm in}(\Delta\omega) = bP_{\rm el}(0)C - aD/[1 + X^2(v_l)]. \quad (30)$$

In effect, $E_{in}(\Delta\omega)$ is an integration over all of the inelastic scattering intensity within the momentum-space volume described by $H(\Delta Q_x, \Delta Q_y)V(\Delta Q_z)$.

The reliability of the above calculations can be demonstrated by comparison with experimentally measured quantities. The incident-beam angular parameters are dependent on the size of the source, the size and mosaic of the LiF monochromating filter, and the collimation. For this work, the mosaic of the LiF monochromating filter determines the horizontal incident-beam divergence, with an angular spread of $\alpha_i = 0{\cdot}0012$ rad. The vertical divergence is determined primarily by the height and distance of the source, which give an angular spread of $\beta_i = 0{\cdot}017$ rad, but is complicated by the presence of the monochromating filter, which results in a smaller effective angular spread for a β_i of 0·011 rad. The scattered-beam angular parameters are determined by the detector collimation, which is determined by a slit 2·22 cm high, 0·51 cm wide and 78·7 cm away from the sample, giving $\alpha_f = 0{\cdot}0027$ rad and $\beta_f = 0{\cdot}011$ rad. These parameters can be determined independently by measuring intensity contours for a Bragg reflection. With an LiF crystal, contours measured for a series of reflections with the same instrumental parameters used in the silicon experiments yielded values of $\alpha_i = 0{\cdot}0010$ and $\alpha_f = 0{\cdot}0024$ rad. For the vertical parameters, β_i and β_f cannot be measured separately, but a measurement by tilting the LiF crystal gives a value of 6·9 Å^2 for the parameter M_{33}.

The coherent scattering cross section may be described as a sum of elastic and one or more phonon

processes (Willis, 1969; Cochran, 1966). The one-phonon cross section may be written

$$(\mathrm{d}^2\sigma/\mathrm{d}\omega\,\mathrm{d}\Omega)_1 = |F(\mathbf{Q})|^2 \sum_{j=1}^{3n} |\mathbf{Q}\cdot\mathbf{e}_j(\mathbf{q})|^2 \times [E_j(\mathbf{q})/m\omega_j^2(\mathbf{q})][(2\pi)^3/V_{\mathrm{cell}}] \times \delta(\mathbf{Q}-\mathbf{G}-\mathbf{q})\delta(\omega-\omega_j), \quad (31)$$

where

$$F(\mathbf{Q}) = \sum_{l=1}^{n} f_l(\mathbf{Q}) \exp(i\mathbf{Q}\cdot\mathbf{r}_l) \exp[-W_l(\mathbf{Q})]$$

is the structure factor for the reciprocal-lattice point $\mathbf{G}$, $\mathbf{q}=\mathbf{Q}-\mathbf{G}$ is the vector from the reciprocal-lattice point, V_{cell} is the unit-cell volume and m is the atomic mass. The $e_j(\mathbf{q})$ are the three phonon polarization vectors, $\omega_j(\mathbf{q})$ are the phonon frequencies, and $E_j(\mathbf{q}) = (h/2\pi)\omega_j(\mathbf{q})(\langle n_j\rangle+\frac{1}{2})$ is the total phonon energy in state j. In the structure factor, $f_l(\mathbf{Q})$ is the atomic form factor, $\mathbf{r}_l$ is the position of the lth atom in the unit cell, and $W_l(\mathbf{Q})$ is the Debye-Waller factor. The phonon frequencies near the Bragg peak can be calculated from the elastic constants, which for Si are $C_{11}=1{\cdot}66$, $C_{12}=0{\cdot}64$ and $C_{44}=0{\cdot}80$ (all $\times 10^{11}$ N m^{-2}) (Huntington, 1958).

The expected value of the TDS intensity may be calculated by integrating (33) over the momentum-space volume observed at a given setting. For the silicon calculation at room temperature, the acoustic phonon scattering dominates. For small phonon wave vectors, $(h/2\pi)\omega \ll kT$, which gives $E_j(\mathbf{q}) = kT$. Also, since $q \ll Q$, Q can be taken as a constant, Q^0, and consequently $F(\mathbf{Q}^0)$ is constant. The integral to be evaluated to give the total one-phonon scattering intensity becomes

$$I = \Phi^0|F(\mathbf{Q}^0)|^2/(k^0)^3 \sin 2\theta^0 \times \int \sum_{j=1}^{3} |\mathbf{Q}^0\cdot\mathbf{e}_j(\mathbf{q})|^2[kT/m\omega_j^2(\mathbf{q})] \times R(\Delta\mathbf{Q},\Delta\omega)[(2\pi)^3/V_{\mathrm{cell}}] \times \delta(\mathbf{Q}-\mathbf{G}-\mathbf{q})\delta(\omega-\omega_j)\,\mathrm{d}^3\Delta\mathbf{Q}\,\mathrm{d}\Delta\omega. \quad (32)$$

For the case of a small region near a Bragg reflection at a constant temperature, the variable part of the integrand becomes

$$\sum_{j=1}^{3} |\mathbf{Q}^0\cdot\mathbf{e}_j(\mathbf{q})|^2[1/\omega_j^2(\mathbf{q})] \exp\left(-\tfrac{1}{2}\sum_{kl} M_{kl}\,\Delta Q_k\,\Delta Q_l\right). \quad (33)$$

The integration has been performed numerically by an Euler-MacLaurin summation method for a number of instrument settings in both transverse and longitudinal directions, to show quantitatively how the thermal diffuse scattering depends on $\mathbf{q}$ in these directions. The step sizes were chosen to be small compared with the Gaussian widths of the momentum-resolution function. The phonon frequencies and the polarization vectors were calculated in the long-wavelength limit for each point on the integration grid.

The calculated TDS profiles were compared with the measured intensities by performing a one-parameter (intensity) least-squares fit to the data. In both the transverse (Fig. 2) and longitudinal (Fig. 3) directions, these fitted profiles were in agreement with the data within the experimental uncertainties. Detailed investigation of the dependence of the calculated profile on resolution and the elastic constants revealed that transverse modes propagating in a direction perpendicular to the scattering plane dominated the observed phonon intensity, because of the large acceptance in the vertical direction.

Discussion

This study differed from the earlier extensive Mössbauer studies of silicon TDS (Albanese *et al.*, 1972; Krec & Steiner, 1984) in that the higher intensity available allowed much greater momentum resolution in shape between the elastic Bragg intensity, which is seen in only a very small region of reciprocal space, and the much broader TDS intensity distribution. The TDS in silicon has also been measured in elastic neutron scattering (Graf, Schneider, Freund & Lehmann, 1981) with perfect crystals of varying thickness. This method utilizes the fact that elastic scattering is essentially independent of thickness in the dynamical limit, while the weaker TDS varies with thickness according to the kinematical limit. This technique gave good results, but still at somewhat lower momentum resolution than the present work. The variable-thickness method is limited, however, to materials for which perfect crystals of varying thickness are readily available.

The calculated intensity and distribution of the inelastic scattering is strongly dependent on the size and shape of the momentum-resolution function. In contrast to neutron diffraction, the energy resolution is independent of the momentum resolution, and its slope cannot be varied, for example, to be focusing for transverse acoustic phonon branches. The Mössbauer resolution function is energy focused only when the dispersion surface has zero slope, for example at the zone boundary or for many optic branches. The measured half widths of the momentum-resolution ellipsoid for the silicon 444 of 0·011, 0·11 and 1·13 Å^{-1}, respectively, for ΔQ_x, ΔQ_y and ΔQ_z can be compared with the corresponding values of 0·02, 0·06 and 0·08 Å^{-1} for a typical neutron instrument (Cooper & Nathans, 1967), recalling that the energy and the momentum transfers in neutron scattering are not independent. The vertical resolution is especially poor compared with neutron scattering

because of the short wavelength. This fact at present limits the amount of detail available in the TDS profiles, and direct extraction of the elastic constants is not possible. The vertical resolution can be improved by the incorporation of horizontal Soller slits, such that the observed TDS profiles would fall off more quickly with **q** in both the transverse and longitudinal directions. If the counting-rate reduction were not too severe, this improvement would provide greater detail within the limits of the one-phonon model.

In summary, the analysis of the resolution function for Mössbauer γ-ray scattering presented here has led to a good understanding of the strengths and limitations of this experimental probe. This better understanding is crucial to the interpretation of TDS measurements and of direct measurements of inelastic and quasi-elastic scattering which are planned for the QUEGS instrument.

The authors thank S. A. Werner for suggestions leading to a better understanding of the resolution function.

References

ALBANESE, G., GHEZZI, C., MERLINI, A. & PACE, S. (1972). *Phys. Rev. B*, **5**, 1746-1757.

COCHRAN, W. (1966). *Phonons in Perfect Lattices and Lattices with Point Imperfections*, edited by R. W. H. STEVENSON, pp. 153-160. Edinburgh: Oliver & Boyd.

COOPER, M. J. & NATHANS, R. (1967). *Acta Cryst.* **23**, 357-367.

COOPER, M. J. & ROUSE, K. D. (1968). *Acta Cryst.* A**24**, 405-410.

DOLLING, G. & COWLEY, R. A. (1966). *Proc. Phys. Soc. London*, **88**, 463-494.

GHEZZI, G., MERLINI, A. & PACE, S. (1969). *Nuovo Cimento B*, **64**, 103-115.

GRAF, H. A., SCHNEIDER, J. R., FREUND, A. K. & LEHMANN, M. S. (1981). *Acta Cryst.* A**37**, 863-871.

HUNTINGTON, H. B. (1958). *Solid State Phys.* **7**, 213-351.

KASHIWASE, Y. & MINOURA, M. (1983). *Jpn J. Appl. Phys.* **22**, L49-L51.

KREC, K. & STEINER, W. (1984). *Acta Cryst.* A**40**, 459-465.

LEDERER, C. M. & SHIRLEY, V. S. (1978). *Table of Isotopes*, 7th ed. New York: Wiley.

MULLEN, J. G., DJEDID, A., COWAN, D. L., SCHUPP, G., XIE, Q., CROW, M. L., CAO, Y. & YELON, W. B. (1987). In preparation.

MULLEN, J. G., DJEDID, A., HOLMES, C., SCHUPP, G., CROW, M. L. & YELON, W. B. (1986). *Nucl. Instrum. Methods*, B**14**, 323-340.

MULLEN, J. G. & STEVENSON, J. R. (1978). *AIP Conf. Proc.* **38**, 55-57.

NILSSON, G. & NELIN, G. (1972). *Phys. Rev. B*, **6**, 3777-3786.

NILSSON, N. (1957). *Ark. Fys.* **12**, 247-257.

O'CONNOR, D. A. & BUTT, N. M. (1963). *Phys. Lett.* **7**, 233-235.

SCHNEIDER, J. R. (1974). *J. Appl. Cryst.* **7**, 541-546.

SCHNEIDER, J. R. (1983). *J. Cryst. Growth*, **65**, 660-671.

WERNER, S. A. & PYNN, R. (1971). *J. Appl. Phys.* **42**, 4736-4749.

WILLIS, B. T. M. (1969). *Acta Cryst.* A**25**, 277-300.

YELON, W. B. & ROSS, F. K. (1982). *Nucl. Instrum. Methods*, **193**, 285-295.

YELON, W. B., SCHUPP, G., CROW, M. L., HOLMES, C. & MULLEN, J. G. (1986). *Nucl. Instrum. Methods*, B**14**, 341-347.

Acta Cryst. (1987). A**43**, 645-653

On the Fast Rotation Function

BY JORGE NAVAZA

Laboratoire de Physique, Tour B, Centre Universitaire Pharmaceutique, 92290 *Chatenay-Malabry, France*

(*Received* 5 *February* 1986; *accepted* 2 *April* 1987)

Abstract

An analysis of the mathematical structure of the rotation function is presented. The effect of truncation of the expansions used in the fast rotation function is discussed and an alternative procedure of calculation which drastically reduces the errors is proposed. A method of sampling on spherical surfaces is developed. The rotation function can thus be obtained from the values it takes at the sampling points. The method can also be used to compute expansions in spherical harmonics of Patterson functions restricted to arbitrary domains. Topological properties of the rotation group are used to obtain distortion-free plots of the different sections of the rotation function.

Introduction

In Crowther's formulation of the fast rotation function, emphasis is placed on the expansion of the Patterson functions in terms of the spherical harmonics and the spherical Bessel functions (Crowther, 1972). These expansions lead to slowly convergent series and the relative errors of some contributions can exceed 100% for reflections corresponding to

0108-7673/87/050645-09$01.50